Total Absorption Spectroscopy Study of the Beta Decay of ^{86}Br and ^{91}Rb

S. Rice,[1] A. Algora,[2,*] J. L. Tain,[2] E. Valencia,[2] J. Agramunt,[2] B. Rubio,[2] W. Gelletly,[1] P.H. Regan,[1] A.-A. Zakari-Issoufou,[3] M. Fallot,[3] A. Porta,[3] J. Rissanen,[4] T. Eronen,[4] J. Äystö,[5] L. Batist,[6] M. Bowry,[1] V. M. Bui,[3] R. Caballero-Folch,[7] D. Cano-Ott,[8] V.-V. Elomaa,[4] E. Estevez,[2] G. F. Farrelly,[1] A. R. Garcia,[8] B. Gomez-Hornillos,[7] V. Gorlychev,[7] J. Hakala,[4] M. D. Jordan,[2] A. Jokinen,[4] V. S. Kolhinen,[4] F. G. Kondev,[9] T. Martínez,[8] E. Mendoza,[8] I. Moore,[4] H. Penttilä,[4] Zs. Podolyák,[1] M. Reponen,[4] V. Sonnenschein,[4] A. A. Sonzogni,[10] and P. Sarriguren[11]

[1] *University of Surrey, Department of Physics, Guildford GU2 7XH, United Kingdom*
[2] *Instituto de Fisica Corpuscular (CSIC-Universitat de Valencia), Apdo. Correos 22085, E-46071 Valencia, Spain*[†]
[3] *SUBATECH, CNRS/IN2P3, Université de Nantes, Ecole des Mines, F-44307 Nantes, France*
[4] *University of Jyväskylä, Department of Physics, P.O. Box 35, FI-40014 Jyväskylä, Finland*
[5] *Helsinki Institute of Physics, FI-00014 University of Helsinki, Finland*
[6] *Petersburg Nuclear Physics Institute, RU-188300 Gatchina, Russia*
[7] *Universitat Politecnica de Catalunya, E-08028 Barcelona, Spain*
[8] *Centro de Investigaciones Energéticas Medioambientales y Tecnólogicas, E-28040 Madrid, Spain*
[9] *Nuclear Engineering Division, Argonne National Laboratory, Argonne, Illinois 60439, USA*
[10] *NNDC, Brookhaven National Laboratory, Upton, New York 11973, USA*
[11] *Instituto Estructura de la Materia, IEM-CSIC, Serrano 123, E-28006 Madrid, Spain*

(Dated: February 13, 2017)

The beta decays of ^{86}Br and ^{91}Rb have been studied using the total absorption spectroscopy technique. The radioactive nuclei were produced at the IGISOL facility in Jyväskylä and further purified using the JYFLTRAP. ^{86}Br and ^{91}Rb are considered high priority contributors to the decay heat in reactors. In addition ^{91}Rb was used as a normalization point in direct measurements of mean gamma energies released in the beta decay of fission products by Rudstam *et al.* assuming that this decay was well known from high-resolution measurements. Our results shows that both decays were suffering from the Pandemonium effect and that the results of Rudstam *et al.* should be renormalized.

Beta decay studies can provide relevant information for fundamental physics, nuclear structure and practical applications. One important application is in nuclear technology, where beta decay data are used for the evaluation of γ-ray and β spectra emitted by fission products in a working reactor, after reactor shut down, in the nuclear waste generated and for the prediction of the spectrum of antineutrinos emitted by a reactor [1, 2].

In recent years the summation calculation method is the most widely used technique for the evaluation of the β- and γ- energy released from the fission products in a reactor or in the nuclear waste. The inputs needed for these calculations are the mean- γ and β energies released in the beta decay of each fission product. The mean energies can be obtained from direct measurements of the gamma [3] and the beta [4] radiation emitted in each radioactive decay or can be deduced from evaluated nuclear data available in databases [5]. Most of the data, which are available in databases, come from measurements using conventional high-resolution gamma-ray spectroscopy, that can suffer from a systematic error known as the Pandemonium effect [6]. This systematic error arises from the difficulty of detecting weak γ-ray cascades and (or) high-energy γ-rays with the limited efficiency of germanium detectors that are usually employed in conventional β-decay studies. As a result, the decay scheme deduced may be incomplete, and the beta decay probability distribution, deduced from the gamma intensity balance populating and de-exciting each level, may be incorrect. In practical terms this means erroneously assigning more beta intensity to lower-lying levels and as a consequence leads to an overestimation of the mean beta energies and an underestimation of the mean gamma energies.

To avoid this systematic error, the total absorption gamma-ray spectroscopy technique (TAGS) can be used. The technique aims at detecting gamma cascades rather than individual γ rays using large 4π scintillation detectors. The advantage of this method over high-resolution germanium spectroscopy to locate missing β intensity has been demonstrated before, for cases measured using both techniques and in particular measured with a highly efficient Ge array [7–9].

In this article we present the results of measurements performed for two decays, ^{86}Br and ^{91}Rb, which are considered high priority contributors to the decay heat in reactors [10–12]. Previous results from the same experimental campaign have already been published [13, 14]. The total absorption measurement of the decay of ^{91}Rb is of particular interest, since it was used as a calibration point for the mean gamma energy measurements of Rudstam *et al.* [3]. In the measurements of Rudstam *et al.*,

* Corresponding author:algora@ific.uv.es
† On leave from Institute of Nuclear Research, Debrecen, Hungary

a well collimated NaI(Tl) scintillation detector was used to detect single γ-rays from decay cascades of the mass separated fission products. From the measured spectrum a γ-ray intensity distribution was obtained after deconvolution with the measured spectrometer response. To derive the mean γ energy from this distribution the intensity must be calibrated on an absolute scale. For this, the number of decays was obtained from selected transitions whose intensity was regarded as well known and were detected in an auxiliary Ge(Li) detector. To calibrate the absolute efficiency of the setup ^{91}Rb was selected because it has a relatively large $Q_\beta = 5907(9)$ keV value and the decay level scheme was regarded as being free from Pandemonium. Thus the calibration of the mean gamma energies in Ref. [3] was done using an intensity of 8.3(4)% for the 436 keV transition in ^{91}Sr and matching the mean energy of the ^{91}Rb distribution to the high resolution value of 2335(33) keV. ^{91}Rb was also measured by Greenwood *et al.* [15] using the total absorption technique, but employing different analysis techniques. The present measurement will allow us to compare our data with Greenwood's results to further validate the measurements and the analysis techniques.

The determination of the beta decay probability distribution free from the Pandemonium effect also makes it possible to compare the deduced strength with theoretical calculations. ^{91}Rb lies in a transitional region characterized by shape changes [16]. For that reason it is also worth exploring the possibility of infering its ground state shape from a comparison of the deduced beta strength in the daugther with theoretical calculations as was already performed for nuclei in the A$\sim$80 and A$\sim$190 regions [17–21].

^{86}Br decay is also of particular interest from the perspective of total absorption measurements. It has a large $Q_\beta = 7633(3)$ keV value, and the high resolution decay scheme is poorly known. Only 17 excited levels have been placed in ^{86}Kr while the total number of levels expected to be fed, from level density considerations, is around 300. Thus one could expect a relatively large Pandemonium effect. This and the large contribution of this decay at cooling times around 100 s are the reasons to include this nucleus with high priority in the lists [11, 12] for decay heat data measurements using the TAGS technique.

THE EXPERIMENT

The measurements were performed at the IGISOL facility [22] of the University of Jyväskylä as part of an experimental campaign aimed at measuring beta decays of nuclei that are important contributors to the decay heat and to the antineutrino spectrum in reactors. As already discussed in [13, 14], the isotopes of interest were produced by proton-induced fission of uranium and first mass separated using the moderate resolution mass separator of IGISOL with a mass resolving power of approximately 500. Since the purity of the samples is of great importance for the measurements, the radioactive beam of the selected mass was further purified isotopically using the JYFLTRAP Penning trap [23, 24]. Then, the extracted radioactive beam of the isotope of interest was implanted at the centre of the total absorption spectrometer onto a tape which was moved periodically to reduce the impact of the daughter contamination in the measurements. The measurement cycles were selected according to the half-lives of the decay of interest. Behind the tape, at approximately 5 mm from the implantation point, a 0.5 mm thick Si detector with a β-detection efficiency of about 25% was placed. The implantation point was surrounded by the Valencia-Surrey Total Absorption Spectrometer *Rocinante*. This spectrometer is a cylindrical 12-fold segmented BaF_2 detector with a length and external diameter of 25 cm, and a longitudinal hole of 5 cm diameter. The separation between crystals in this spectrometer is provided by a thin optical reflector. The total efficiency of the setup for detecting a single γ ray is larger than 80% (up to 10 MeV). Since the BaF_2 has an intrinsic background, coincidences with the beta detector were used to generate β-gated TAGS spectra in the present analysis. Using coincidences also avoids the contribution of normal ambient background in the measured spectra.

TABLE I. Level Density parameters used in the analysis for daughter isotopes (parameters given for the Gilbert-Cameron (GC) formulation [29], which is a combination of the Back Shifted Fermi Gas (BSFG) model [30] plus the Constant Temperature (CT) model [31] for high excitation energy). The parameters are: the ground state position Δ, the level density a (for BSFG), nuclear temperature T and the back-shift E_0 (for CT) and the matching point E_x of the BSFG and CT models for the Gilbert and Cameron model

	Level density Parameters				
Isotope	a	Δ	T	E0	Ex
^{86}Kr	8.434	1.599	0.833	1.518	4.342
^{91}Sr	9.754	0.264	0.662	0.425	1.946

ANALYSIS

The first step in the analysis of the total absorption experiments is to determine the contaminats in the spectra to be analyzed. As mentioned earlier, the use of the beta-coincidence conditions, cleans the spectrum of internal and ambient backgrounds, but daughter decay contamination and pulse pileup contributions have to be determined. Since we are dealing with a segmented detector, apart from the electronic pulse pile-up that affects a single detector module [25], one must also consider the summing of signals from different detector modules [14]. To address this problem a new Monte Carlo (MC) procedure to determine their combined contribution has been implemented. The method is based on the random superposition of two of the stored events within the analog to digital converter (ADC) gate length. The normalization of the resulting summing-pileup spectrum is then calculated by the event rate and the ADC gate length as in Ref. [25]. Once the contributions of the contaminants have been determined, one can apply the analysis methods to the measured spectrum to obtain the feeding distribution. In this work as in earlier studies, we follow the procedures developed by the Valencia group [26, 27].

For that we need to solve the TAS inverse problem:

$$d_i = \sum_{j=0}^{j_{max}} R_{ij}(B) f_j + C_i \quad (1)$$

where d_i is the content of bin i in the measured TAS spectrum, R_{ij} is the response matrix of the TAS setup and represents the probability that a decay that feeds level j in the level scheme of the daughter nucleus gives a count in bin i of the TAS spectrum, f_j is the beta feeding to the level j and C_i is the contribution of the contaminants to bin i of the TAS spectrum. The response matrix R_{ij} depends on the TAS setup and on the assumed level scheme of the daughter nucleus (branching ratio matrix B). To calculate the response matrix the B matrix for the levels in the daughter nucleus has to be determined first. For that the level scheme of the daughter nucleus is divided into two regions, a low excitation part and a high excitation part. Conventionally the levels of the low excitation part and their gamma decay branchings are taken from high resolution measurements available in the literature, since it is assumed that the gamma branching ratios of these levels are well known. Above a certain energy, the cut energy, a continuum of possible levels divided in 40 keV bins is assumed. From this energy up to the decay Q value, the statistical model is used to generate a branching ratio matrix for the high excitation part of the level scheme. The statistical model is based on a level density function and gamma strength functions of E1, M1, and E2 character. In the cases presented here, the parameters for the gamma strength function were taken from [28] and the parameters of the level density function [29–31] were obtained from fits to the data available in [28, 32, 33]. Details of the parameters used are given in Tables I and II. As part of the optimisation procedure in the analysis, the cut off energy and the parameters of the statistical model can be changed. Once the branching ratio matrix is defined, the R_{ij} can be calculated recursively from responses previously determined using Monte Carlo simulations [25, 34, 35]. The Monte Carlo simulations were validated with measurements of the spectra of well known radioactive sources (^{24}Na, ^{60}Co, ^{137}Cs). Once the R response matrix is obtained, the Expectation Maximisation (EM) algorithm is applied to extract the beta feeding distributions from equation 1.

The feeding distributions obtained from the analyses will then be used to calculate the mean gamma and beta energies released in the decay using the following relations: $\overline{E_\gamma} = \sum_i E_i * I_i$, and $\overline{E_\beta} = \sum_i I_i * < E_\beta >_i$, where E_i is the energy of the level i, I_i is the normalized feeding to level i, and $< E_\beta >_i$ is the mean energy of the beta continuum populating level i. In the case of ^{91}Rb decay, the normalized feeding distribution will also be used to deduce the beta strentgh for comparison with theoretical calculations.

DECAY OF ^{91}RB

The tape cycle for the measurement of the decay of ^{91}Rb was set to 174.8 s. With this measuring cycle the daughter decay contamination can be estimated to be approximately 0.1 % from the solution of the Bateman equations using 58.2(3) s [36] for the decay half-life of ^{91}Rb, and 9.65(6) h for the half-life of the daughter ^{91}Sr. For that reason the daughter activity was not measured separately. In this case the only contamination in the beta-gated spectrum is the summing-pileup, as showed in Fig. 1.

For the analysis we need to define the branching ratio matrix of the daughter nucleus level scheme. As mentioned earlier this requires the combination of the known levels from high resolution measurements and complementing the missing information up to the Q value with the statistical model. According to the latest ENSDF evaluation [36] the level scheme of the daughter nucleus is poorly known in terms of spin-parity assignments, since only one level in the daughter nucleus has a firm spin-parity assignment in the decay level scheme. The missing spins and parities of the levels needed to be estimated. For that purpose, the known gamma transitions between levels were used in combination with the expectation that most gamma transitions will occur via the most probable E1, E2 and M1 gamma ray transitions, resulting in a range of options available for the missing spins and parities. A number of these levels are recorded to decay via E2/M1 transitions to the 94 keV ($3/2^+$) state, resulting in the initial decaying level probably being $1/2^+$, $3/2^+$ or $5/2^+$. In addition, the beta decay feeding distribution available in ENSDF was also used initially when postulating options for the spin-parity assignments. The large number of degrees of freedom now available via these options results in a range of level schemes. These level schemes were considered up to different energy level thresholds for the application of the statistical model during the analysis.

The parameters used in the final analysis for the level density parametrization and for the gamma strength functions are given in Tables I and II. For the continuum part of the level scheme several possibilities were tested for the level density parametrization (Back Shifted Fermi Gas formula, Constant Temperature and a combination of both, the Gilbert Cameron formula [29–31]). Similar results were obtained in the analysis for the Gilbert-Cameron formula and for the Constant Temperature model. In many of the analyses performed it was found that low cut energies in the known level scheme part re-

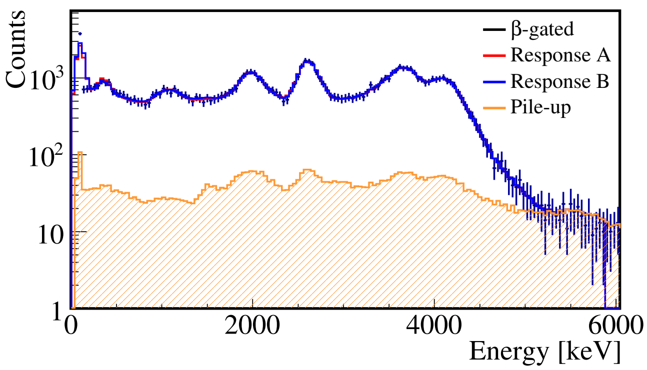

FIG. 1. (Color online) Relevant histograms for ^{91}Rb decay: measured spectrum (dotted line), summing-pileup contribution (green line), reconstructed spectrum response A (red line), reconstructed spectrum response B (blue line) . Response A corresponds to the conventional analysis. Response B has additional optimization on the branching ratio matrix to reproduce the measured γ intensities in high resolution experiments.

sulted in a poor reproduction of the peak around 2600 keV in the total absorption spectrum. It is worth noting that the spin and parity of the parent ^{91}Rb is $3/2^{(-)}$ [36] , for that reason also analyses were performed assuming a $3/2^{+}$ assignment, and considering accordingly other ranges of populated states (allowed and first forbidden decays) that in the case of $3/2^{-}$ ground state assumption. Those analyses provided a poorer reproduction of the data. As a result, in the final accepted analysis, we have assumed a cut energy at 2680 keV and allowed and first forbidden decays were considered assuming a parent state with $3/2^{-}$. The results of the present accepted analyses are presented in Figs. 1 and 2. In Fig. 1 two analyses are provided. Analysis labelled A, represents the analysis performed conventionally. Analysis B, is an analysis performed using a slightly modified branching ratio matrix, in order to reproduce the experimental gamma intensities obtained in high-resolution experiments. This optimization is performed adjusting the gamma feeding from the levels in the continuum to the discrete levels in the branching ratio matrix of the accepted analysis (labelled A). In Table V of the appendix we provide both accepted feeding distributions for comparison. The results presented in Figs. 1 and 2 show that the quality of the reproduction of the measured decay spectrum is very similar for both analyses. Small differences appear in the feeding distribution, as can be seen in Fig. 2, which appear mainly for levels that have direct gamma connections to the ground state. The analysis B is able to reproduce the gamma intensity de-exiting the level 439 within 3 %, which is relevant in this context because the gamma ray of 345.5 keV de-exiting this level, with an intensity error of 5 % was used as the global normalization point by Rudstam *et al.* in their mean gamma energy measurements.

Both feeding distributions obtained are similar to the one obtained by Greenwood [15]. From the two distributions, the feeding distribution obtained with optimized branching ratio matrix lies closer to the Greenwood result. The three total absorption results clearly differ from the ENSDF data [36] based on high resolution measurements. From our conventional analysis a ground state feeding of 10.2 % is obtained, which can be compared with the value of Greenwood *et al.* [**?**] of 6.2 %, the optimized branching ratio matrix result is slightly smaller at 9.2 %. Those values can be compared with the ENSDF adopted value of 2 (5) % [36]. But we must mention that the division of the feeding values between ground state and first excited level at 93.4 keV should be taken with caution, since the two levels lie very close in energy as already presented in Greenwood *et al.* [15]. As an additional test, we also performed an analysis fixing the ground state and first state feeding to the Greenwood values. In this last case the quality of the fit to the data was clearly much worse than the accepted ones.

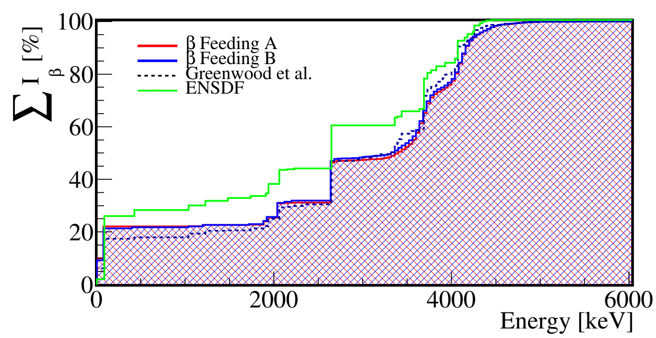

FIG. 2. (Color online) Comparison of the accumulated feeding distributions obtained in this work for the decay of ^{91}Rb with the distributions from earlier high resolution measurements [36] and with that obtained by Greenwood *et al.* [15].

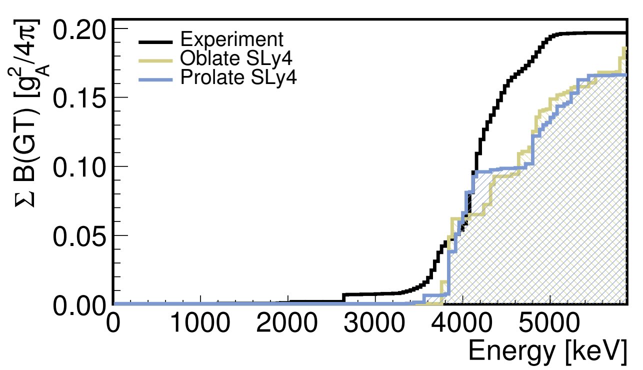

FIG. 3. (Color online) Accumulated strength of the decay of ^{91}Rb compared with QRPA calculations assuming oblate and oblate shapes for the ground state of ^{91}Rb.

In Table III we present a comparison of the deduced mean energies from the present work with the values determined from the Greenwood data and with the value used by Rudstam *et al.* In the table we quote the mean energies deduced from the results obtained from the optimized branching ratio matrix analysis (analysis B). The error in the mean energies is evaluated from the differences in the mean gamma and beta values obtained from several analyses, that provided a good description of the experimental data. The present value is close to the result of Greenwood and shows a large difference with the value used by Rudstam, which was based on earlier high resolution measurements. This result as well as the comparison presented in Fig. 2 confirm that the value used by Rudstam as a normalization point, suffered from the Pandemonium effect. For that reason all mean gamma energies published in Rudstam *et al.* require a renormalization of 1.14.

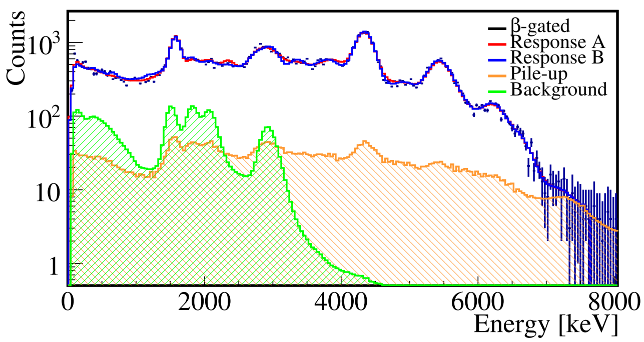

FIG. 4. (Color online) Relevant histograms for ^{86}Br decay: measured spectrum (points with errors), reconstructed spectrum response A (blue line), reconstructed spectrum response B (red line) summing-pileup contribution (red line), background (green line).

As mentioned in the introduction ^{91}Rb lies in a region of shape transitions. For that reason it is also worth examining how well the beta decay strength of ^{91}Rb is reproduced by theoretical calculations that assume different possible shapes for its ground state. The measured strength is compared in Fig. 3 with results from deformed quasiparticle random-phase approximation (QRPA) calculations. In this formalism, a selfconsistent quasiparticle basis is first constructed from deformed Skyrme Hartree-Fock calculations with pairing correlations in the BCS approximation. We use the interaction SLy4 as a representative of the Skyrme forces because of its reliability and predictive power, which is the result of being extensively and successfully tested all over the nuclear chart. Then, we introduce a separable spin-isospin residual interaction in both particle-hole and particle-particle channels with parameters determined phenomenologically in this mass region, which is treated in the QRPA [37].

The total energy as a function of the quadrupole deformation parameter shows two minima, one oblate at $\beta = -0.12$, which is the ground state, and another prolate at $\beta = 0.10$ at about 300 keV excitation energy. The minima are very shallow with practically no barrier between them.

When the decaying nucleus has an odd number of nucleons, the ground state is expressed as a one-quasiparticle state in which the odd nucleon occupies the single-particle orbital of lowest energy. We use here the equal filling approximation, treating the unpaired nucleon on an equal footing with its time-reversed state. Experimentally, the assignment of spin-parity for the ground state of ^{91}Rb is $J^\pi = 3/2^-$, whereas an excited state $J^\pi = 5/2^-$ is observed at 108 keV. These assignments are chosen for the oblate ground state and prolate excited state in ^{91}Rb, respectively. They correspond to single-particle states found in the vicinity of the proton Fermi level.

Two types of transitions can be considered in the decay of odd-A nuclei. One of them is due to phonon excitations in which the odd nucleon is a spectator. In the intrinsic frame, the GT transition amplitudes are similar to those in the decay of the even-even case, but with the blocked spectator excluded from the calculation. The other type of transitions involves the odd-nucleon state. The former excitations correspond to three quasiparticle (3qp) states and appear at excitation energies above twice the pairing gap energies, typically 2-3 MeV. The latter are one quasiparticle (1qp) excitations and appear in the low-lying spectrum as well.

Figure 3 shows the accumulated Gamow-Teller strength for the oblate and prolate shapes of ^{91}Rb calculated in QRPA with the force SLy4. A standard quenching factor $(g_A/g_V)_{\rm eff} = 0.77(g_A/g_V)$ is included in the calculations to compare with the data. In general, the agreement with experiment is very reasonable. There is basically no strength at low energy. The strength is concentrated at around 4 MeV and 5 MeV in the calculations. It is more fragmented and spread in the experiment, but again concentrated at about 4 MeV. The total strength contained in the Q_β energy window is also comparable, although somewhat underestimated. It is also worth mentioning the similarity between the strength distributions of both oblate and prolate shapes that would prevent in this case the use of these experiments to determine deformation. The absence of GT strength observed in the calculations below 3-4 MeV is understood from the fact that the formalism deals only with allowed GT transitions. Indeed, the neutron states close to the neutron Fermi level are immersed in the group of states split from the spherical shells $g_{7/2}$ and $d_{5/2}$, which are positive parity states that cannot be connected with allowed transitions with the negative parity states coming from the $f_{5/2}$ and $p_{3/2}$ shells located in the vicinity of the proton Fermi level. Thus, most probably, the observed strength in the low-lying excitation energy has its origin in forbidden transitions involving a change in the parity of the states, which are not included in calculations in the present formalism.

DECAY OF ^{86}BR

The β^- decay of ^{86}Br proceeds to the stable nucleus ^{86}Kr, therefore daughter contamination is not a problem for this decay. As in the ^{91}Rb case, the pileup was calculated according to the recently developed procedure [14]. A preliminary analysis of the spectra cleaned of pileup highlighted that there is a small amount of contamination in the beta gated spectra. Since the production of the isotope was continuously checked and pure, the contamination was identified as a small background contribution, due to an increased level of noise in the silicon detector in one of the runs. Possible solutions to eliminate this contamination are the exclusion of the run from the analysis or to increase the threshold of the silicon detector, but since this run contained an important part of the statistics, we decided to use an alternative solution. In the analysis of this case we have subtracted from the beta-gated spectrum a background spectrum with beam-on, from which its own pileup had been previously subtracted. The level of subtraction was determined from a comparison with the clean run. The resulting spectra, with all the contributions are presented in Fig. 4, where the results of the reconstructed spectra after the analyses are also shown.

The first step in the deconvolution process is the determination of the branching ratio matrix. As discussed in the ^{91}Rb case, the three statistical models (GC, BSFG and CT [29–31]) were fitted to the mixture of experimental and theoretical data to obtain the relevant level density parameters. Those resulting from the GC model are summarised in Table I. Also in Table II the gamma strength parameters used in the construction of the branching ratio matrix for the daughter isotope ^{86}Kr are provided.

The level scheme of the daughter ^{86}Kr is better known than in the ^{91}Sr case. Up to the level at an excitation energy of 3099 keV, only two levels have uncertain spin-parity assignments. In addition, a recent ENSDF evaluation [38] has included some new levels from a $^{86}Kr(n,n')^{86}Kr$ study from Fotiades *et al* [39] and slightly revised the excitation energies of some levels compared with the earlier evaluation [40].

An important change in the new evaluation of the decay of ^{86}Br is the new spin-parity assignment of the ground state. Previously the spin-parity assignment of this state was $J^\pi = 2^-$, based on the systematics from $^{82-84}$Br, but a relatively recent study by Porquet *et al.* [41] suggested a possible 1^- asignment arising from the lowest energy state in the $\pi p_{3/2} \nu d_{5/2}$ multiplet. This new value has been assigned to the ground state in the new ENSDF evaluation [38]. In our analyses both options were used, the 1^- cases providing better fits of the total absorption data, in particular to the region of the spectra around the peak at 2250 keV state and in the region between 3500 and 4000 keV. The 2^- analyses also provided a larger ground state feeding value (18.8 % for the conventional analysis) compared with the high resolution results (15(8) %) when allowed and first forbidden transitions are considered.

The final accepted analyses were performed using the 1^- assignment for the parent ground state and a cut energy in the known level scheme at 3560 keV. Allowed and first forbidden transitions were considered. The results of those analyses are presented in Figs. 4 and 5. As in the ^{91}Rb case in Fig. 4 two analyses are provided. Analysis labelled A, represents the analysis performed conventionally. Analysis B, is an analysis performed using a slightly modified branching ratio matrix, in order to reproduce the experimental gamma intensities obtained in high-resolution experiments. In this particular decay the result from the conventional analysis (labelled A) gave a larger discrepancy (41 %) in the reproduction of the gamma intensity from the first excited state when compared with high resolution measurements. After the optimization of the branching ratio matrix, (analysis B), the gamma intensity de-exiting the first excited state is reproduced within 5 %. In Table VI of the appendix both accepted feeding distributions are provided for comparison. The results presented in Figs. 4 and 5 show that the quality of the reproduction of the measured decay spectrum is very similar for both analyses, being slightly worse for the adjusted one. Compared to the ^{91}Rb case, slightly larger differences appear in the feeding distributions, as can be seen in Fig. 5, in particular analysis B, with the optimized branching ratio matrix, provides a larger ground state feeding value. As in ^{91}Rb case, the two total absorption results clearly differ from the ENSDF data [38] based on high resolution measurements, which points to a decay suffering from the Pandemonium effect. From our conventional analysis (analysis A) a ground state feeding of 15.01 % is obtained, the optimized branching ratio matrix analysis result is larger, amounting to 20.23 % , but still in agreement with the ENSDF value within the error interval (15 (8) %). The ground state value of the optimized branching ratio matrix analysis agrees better with the recently published preliminary results of Fijałkowska *et al.* [42] that also use the total absorption technique, which show a value above 20 %. Our analyses also provide no feeding to levels at 2250 keV (4^+) and at 2350 keV (2^+), also pointing to possible Pandemonium effect affecting these levels, when compared with the high resolution results.

In Table IV we present a comparison of the deduced mean energies from the present work with the values obtained from high resolution measurements. As in the ^{91}Rb case, we provide the value obtained from the optimized branching ratio analysis result. The value obtained for the electromagnetic component is 358 keV smaller than the preliminary values obtained by Fijałkowska *et al.* [42] (4110 (411) keV) determined with a large uncertainty. In this last publication [42] no details of the specific assumptions for the analysis of this decay were given, so we can not discuss further the possible sources of differences with our analysis.

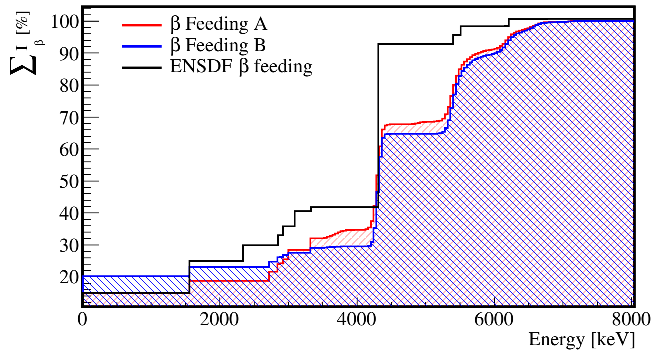

FIG. 5. (Color online) Comparison of the accumulated feeding distributions obtained in this work for the decay of ^{86}Br with the distributions from earlier high resolution measurements [38].

DISCUSSION AND CONCLUSIONS

This work has presented the study of the beta decay of ^{86}Br and ^{91}Rb using the total absorption technique. Both decays were considered to be important contributors to the decay heat in reactors [10–12] and were shown to suffer from the Pandemonium effect. The decays were studied using isotopically pure beams provided by the IGISOL facility using the JYFL Penning trap and a recently developed total absorption detector. The decay of ^{91}Rb is of particular interest, because this decay was used as a normalization point in the systematic studies of Rudstam *et al.* [3], where it was assumed that this decay does not suffer from the Pandemonium effect. This decay was also measured by Greenwood *et al.*, [15] so it is possible to compare both TAS results and establish possible systematic differences arising from the different analysis techniques used. On one hand our present results for ^{91}Rb agree quite well with the results of Greenwood *et al.*. On the other hand the deduced gamma mean energy associated with this decay differs from the high resolution value used by Rudstam *et al.* pointing to the necessity of renormalizing the gamma energies of this work.

It was pointed out by O. Bersillon in one of the earlier meetings of the WPEC25 [10, 11], that there are large discrepancies between the mean energies deduced from the TAS results of Greenwood and the Rudstam results. In particular, the Rudstam mean gamma energies are systematically smaller than the corresponding mean energies deduced from the Greenwood TAS data. One might think that the source of the discrepancy lies in the incorrect normalization value. So, this is an issue that can be revisited using the new normalization of the Rudstam data set presented in this article. In the comparison presented here we have also included the mean energies deduced for some cases of our recent TAS work for which the differences with Rudstam data can be calculated (^{86,87,88}Br, ^{91,92,94}Rb [13, 14, 43]). The comparison is presented in Fig. 6 first using the original Rudstam results and then in Fig. 7 using the renormalized results of Rudstam with our present value of the mean gamma energy of ^{91}Rb decay. The results show that even though the relative differences are reduced, there is a remaining systematic difference between the two data sets. The mean value of the differences in the mean gamma energies changes from -360 keV to -180 keV after the renormalization by 1.14. In any case the most striking fact is the large spread of the observed differences ranging from -0.8 MeV to $+0.6$ MeV even after the normalization. There seems to be no systematic trend. At present the origin of such discrepancies is not clear.

It is also possible to deduce the beta spectrum from the TAS data for both measured cases and compare with the measurements of Tengblad *et al.* [3, 4]. This comparison is also relevant because one of the cross-checks employed in Rudstam's publication is the comparison of the sum of the mean gamma, beta and deduced antineutrino mean energies with the Q value of the decay. If there is a systematic difference in the mean gamma energies, we can expect possible systematic differences also in the beta decay energies and in the deduced beta spectra. This is presented in Fig. 8 for ^{91}Rb decay and in Fig. 9 for the ^{86}Br decay. The beta spectrum has been deduced assuming allowed shape transitions and using the subroutines of the program LOGFT of the NNDC (Brookhaven) [44]. We see systematic differences in the beta spectrum of both decays. These differences can not be explained by the assumption of the allowed character of the beta transitions used in the deduction of the spectra from the TAS measurements. Actually if we assume first forbidden transitions (using the procedure employed in the LOGFT utility of NNDC) for all beta transitions the deduced beta spectrum does not differ so much from the one obtained assuming allowed transitions and presented here [45]. For the present cases and for the recently studied ^{87,88}Br and ^{94}Rb cases [43] we can see that the deduced beta spectrum from TAS measurements is systematically softer (shifted to lower energies) than the directly measured Tengblad data [4]. This can be an important issue to be taken into account for antineutrino summation calculations using different data sets.

The relative impact of the TAS data of both decays on the calculations of the decay heat and on the predictions of the antineutrino spectrum is compared in Figs. 10, 11 and Figs. 12, and 13 with respect to high resolution data (taken from ENDF/BVII.1, that did not include TAS data). They have a small impact on the decay heat calculations and it is more relevant for ^{235}U than for ^{239}Pu. As can be seen in Fig. 10 it amounts to up to 0.5 % in ^{235}U and up to 0.2 % in ^{239}Pu for the electromagnetic component. The contribution to the light particle component is approximately 0.2 % for ^{235}U and 0.1 % for ^{239}Pu at its maximum. As in the case of the decay heat, the impact on the antineutrino spectrum is more relevant for ^{235}U and for all fuels (^{235}U, ^{238}U, ^{239}Pu, ^{241}Pu) it has the largest contributions at approximately 4 and 7 MeV antineutrino energies, but in opposite directions. At around 3-4 MeV the contribution to the global antineutrino spectrum is reduced in all fuels. At higher enegies (above 6 MeV) the contribution is larger and positive and it comes only from the decay of ^{86}Br that has a larger decay Q value. This latter impact is due to the change in the ground state feeding and affects a region which has partial overlap with the anomaly seen in the antineutrino spectrum centered around 5 MeV [46]. But it must be mentioned that the relative impact of this decay is modest.

The relative limited impact of the presented results in both decay heat and neutrino physics migth seem contradictory with the fact mentioned in the introduction that these decays are considered of high relevance for reactor applications. One must emphasize, that it is only the relative impact of new TAS data in relation with the high resolution data which is modest. Both decays are important contributors to the decay heat in the cooling time range of 100 s, as can be seen in the reactor decay heat calculations presented by M. Fleming and J. C Sublet in [47]. The contributions of the ^{86}Br and ^{91}Rb decays can amount up to 3.9 % and 8.9 % respectively in the gamma component of the decay heat in ^{235}U and up to 1.7 % and 4.2% respectively in ^{239}Pu.

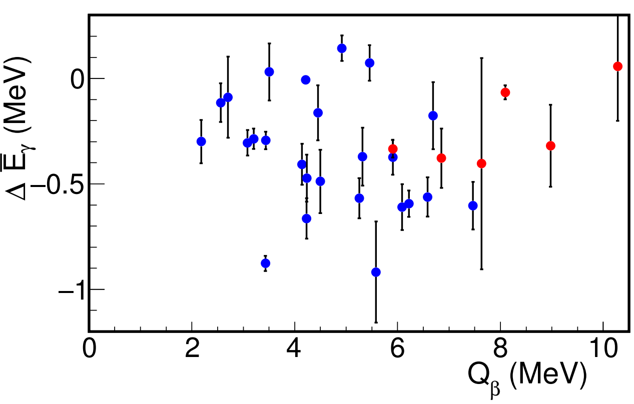

FIG. 6. (Color online) Differences between the mean energies reported in Rudstam *et al.* [3] work and the deduced mean gamma energies from the work of Greenwood *et al.* [15] and our recent data (in red) [13, 14, 43].

This work was supported by Spanish Ministerio de Economía y Competitividad under grants FPA2008-06419, FPA2010-17142 and FPA2011-24553 and FPA2014-52823-C2-1-P, CPAN CSD-2007-00042 (Ingenio2010), and the program Severo Ochoa (SEV-2014-0398) and by EPSRC and STFC (UK). Work at ANL was supported by the U.S Department of Energy under contract DE-AC02-06CH11357. The authors would like to thank the late Olivier Bersillon for drawing our attention to the discrepancy between the mean energies deduced from Greenwood TAS data and the Rudstam data.

[1] A. Algora *et al.*, Phys. Rev. Lett. **105**, 202501 (2010).
[2] M. Fallot *et al.*, Phys. Rev. Lett. **109**, 202504 (2012).
[3] G. Rudstam *et al.*, Atomic Data and Nuclear Data Tables **45**, 239 (1990).
[4] O. Tengblad *et al.*, Nucl. Phys. A 503, 136 (1989).
[5] ENSDF, http://www.nndc.bnl.gov/ensdf
[6] J. Hardy *et al.*, Phys. Lett. B **71**, 307 (1977).
[7] A. Algora *et al.*, Nucl. Phys. A **654**, 727c (1999).
[8] Z. Hu *et al.*, Phys. Rev. C **60**, 024315 (1999).
[9] A. Algora *et al.*, Phys. Rev. C 68, 034301 (2003).
[10] A. L. Nichols, *et al.*, Beta decay and decay heat, INDC(NDS)-0499 (2006)
[11] T. Yoshida *et al.*, Assessment of Fission Product Decay Data for Decay Heat Calculations, OECD/NEA Working Party for International Evaluation Co-operation, Volume 1425 25, 2007.
[12] M. Gupta *et al.*, Decay Heat Calculations: Assessment of Fission Product Decay Data Requirements for Th/U Fuel, IAEA report INDC(NDS)-0577, 2010.
[13] A.-A. Zakari-Issoufou *et al.*, Phys. Rev. Lett. **115**, 102503 (2015)
[14] J. L. Tain *et al.*, Phys. Rev. Lett. **115**, 062502 (2015)
[15] R. C. Greenwood, R. G. Helmer, M. H. Putnam and K. D. Watts, Nucl. Instrum. Methods Phys. Res. A, **390**, 95 (1997)
[16] R. Rodriguez-Guzman, P. Sarriguren, and L. M. Robledo, Phys. Rev. C 82, 061302(R) (2010)
[17] E. Nácher *et al.*, Phys.Rev. Lett. 92, 232501 (2004).
[18] E. Poirier *et al.*, Phys. Rev. C 69, 034307 (2004).
[19] A. Pérez-Cerdan *et al.*, Phys. Rev. C 84, 054311 (2011).
[20] J. A. Briz *et al.*, Phys. Rev. C92, 054326 (2015)
[21] M. E. Estévez Aguado *et al.*, Phys. Rev. C 92, 044321 (2015)
[22] J. Äystö, Nucl. Phys. A **693**, 477 (2001).
[23] V. Kolhinen *et al.*, Nucl. Instrum. Methods Phys. Res. A

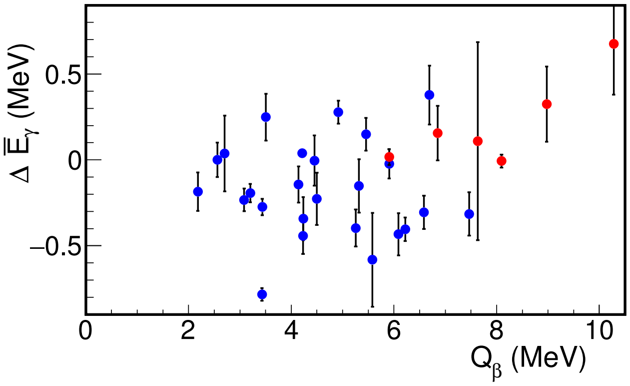

FIG. 7. (Color online) Same as Fig. 6 but renormalizing the mean energies reported in Rudstam *et al.* [3] by the 1.14 value deduced in this work.

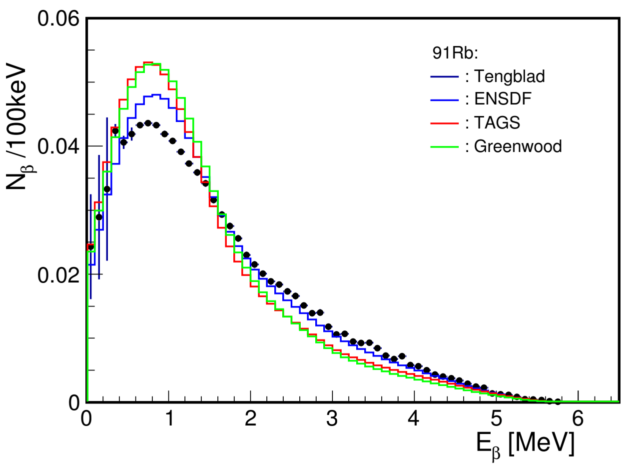

FIG. 8. (Color online) Comparison of the beta spectrum deduced from our TAS measurements, Greenwood measurements and from ENSDF, assuming allowed transitions, with the measurements of Tengblad *et al.* [4]

.

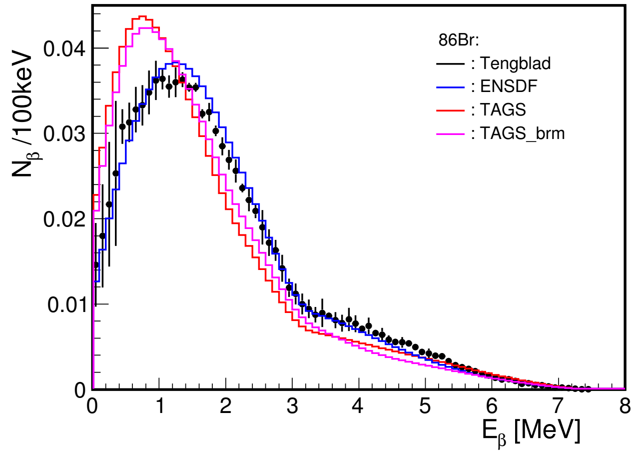

FIG. 9. (Color online) Comparison of the beta spectrum deduced from our TAS measurements for both analyses presented in this work, and from ENSDF, assuming allowed transitions, with the measurements of Tengblad *et al.* [4]

.

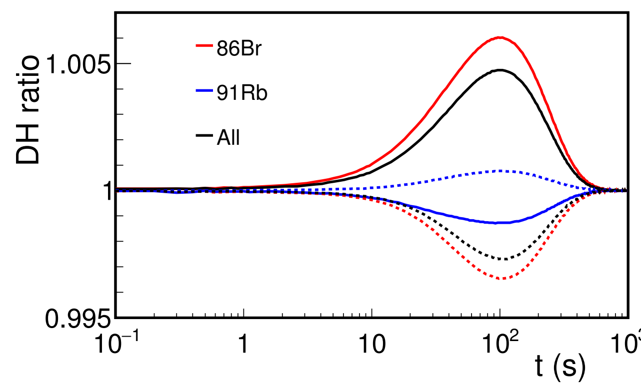

FIG. 10. (Color online) Relative impact of the measured decays on the decay heat of ^{235}U. The continuous line represents the electromagnetic component, the dotted line the light particle component

.

528, 776 (2004).
[24] T. Eronen *et al.*, Eur. Phys. J. A **48**, 46 (2012).
[25] D. Cano-Ott *et al.*, Nucl. Instrum. Methods Phys. Res. A **430**, 488 (1999).
[26] J. L. Tain *et al.*, Nucl. Instrum. Methods Phys. Res. A **571**, 719 (2007).
[27] J. L. Tain *et al.*, Nucl. Instrum. Methods Phys. Res. A **571**, 728 (2007).
[28] RIPL-3, R. Capote *et al.*, Nucl. Data Sheets **110**, 3107 (2009).
[29] A. Gilbert and A. G. W. Cameron. Canadian Journal of Physics **43** 1446 (1965).
[30] W. Dilg, W. Schantl, H. Vonach, and M. Uhl. Nuclear Physics A **217** 269 (1973).
[31] T. Von Egidy, H.H. Schmidt, and A.N. Behkami. Nuclear Physics A **481** 189 (1988).
[32] S. Goriely, F. Tondeur, and J. Pearson, At. Data Nucl. Data Tables **77**, 311 (2001).
[33] P. Demetriou and S. Goriely, Nucl. Phys. A **695**, 95 (2001).
[34] D. Cano-Ott *et al.*, Nucl. Instrum. Methods Phys. Res., Sect. A **430**, 333 (1999).
[35] S. Agostinelli *et al.*, Nucl. Instrum. Methods Phys. Res. A **506**, 250 (2003).
[36] C. M. Baglin, Nuclear Data Sheets **114**, 1293 (2013).
[37] P. Sarriguren, E. Moya de Guerra, and A. Escuderos, Phys. Rev. C 64, 064306 (2001); P. Sarriguren, Phys. Rev. C 79, 044315 (2009).
[38] A. Negret and B. Singh, Nuclear Data Sheets **124**, 1 (2015).
[39] N. Fotiades, M. Devlin, R. O. Nelson, and T. Granier, Phys. Rev. C **87**, 044336 (2013).
[40] B. Singh, Nuclear Data Sheets **94**, 1 (2001).
[41] M.-G. Porquet, *et al.*, Eur. Phys. Journal A **40**, 131

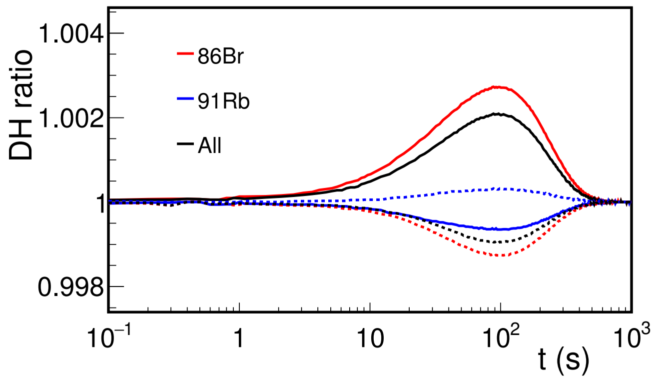

FIG. 11. (Color online) Relative impact of the measured decays on the decay heat of ^{239}Pu (for details see Fig. 10).

.

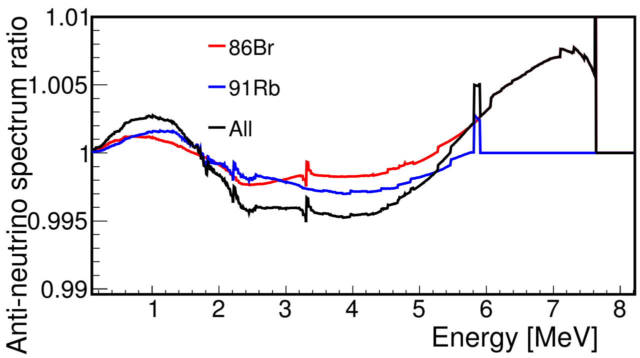

FIG. 12. (Color online) Relative impact of the measured decays on the antineutrino spectrum of ^{235}U

.

(2009).
[42] A. Fijalkowska *et al.*, Acta Phys. Polonica B **45**, 545 (2014).
[43] E. Valencia *et al.*, submitted to Physical Review C.
[44] ENSDF Analysis Programs - LOGFT, National Nuclear Data Center, Brookhaven National Laboratory, http://www.nndc.bnl.gov/nndcscr/ensdf pgm/analysis/logft/
[45] A. Algora *et al.*, contribution to the ND2016 conference, in print
[46] J. H. Choi *et al.*, Phys. Rev. Letts. 116, 211801 (2016) Sheets **112**, 2887 (2011).
[47] M. Fleming and J.-C. Sublet, CCFE-R(15)28/S1 Report, June 2015.

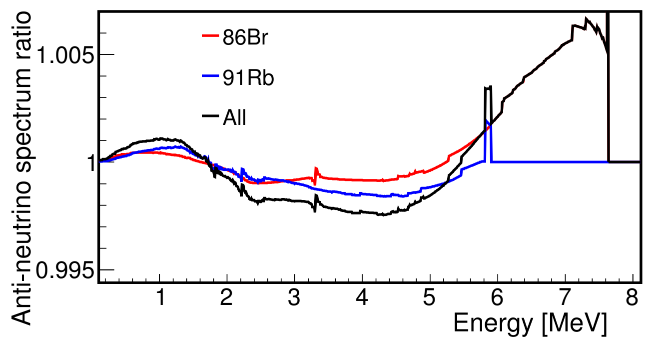

FIG. 13. (Color online) Relative impact of the measured decays on the antineutrino spectrum of ^{239}Pu

.

TABLE II. Gamma strength function parameters used in the analysis for daughter isotopes.

Isotope	E1 Energy [MeV]	E1 Width [MeV]	E1 σ [mb]	M1 Energy [MeV]	M1 Width [MeV]	M1 σ [mb]	E2 Energy [MeV]	E2 Width [MeV]	E2 σ [mb]
^{86}Kr	16.29 17.17	5.37 5.94	178.7 161.63	9.30	4.00	19.67	14.29	5.08	1.78
^{91}Sr	16.08 16.95	5.24 5.79	193.81 175.32	9.13	4.00	2.66	14.03	5.02	1.89

TABLE III. Mean average energy for β-particles and γ rays (all collected photons) from the decay of ^{91}Rb. The ENSDF adopted values are taken from Rudstam *et al.* [3] .

	$\bar{E}_\gamma$ [keV]	$\bar{E}_\beta$ [keV]
Present result	2669(29)	1389(22)
Greenwood *et al.*	2708(76)	1367(44)
ENSDF	2335(33)	1560(30)

TABLE IV. Mean average energy for β-particles and γ rays (all collected photons) from the decay of ^{86}Br.

	$\bar{E}_\gamma$ [keV]	$\bar{E}_\beta$ [keV]
Present result	3782(54)	1687(28)
ENSDF	3296	1944

TABLE V. Feeding distibution obtained for the decay of ^{91}Rb (for details see the text).

E [keV]	Feeding (a) [%]	Feeding (b) [%]	E [keV]	Feeding(a) [%]	Feeding (b) [%]
0.0	10.02	9.21	3100	0.08	0.12
94	12.06	12.11	3140	0.07	0.10
439	0.00	0.46	3180	0.07	0.10
994	0.00	0.00	3220	0.11	0.13
1042	0.13	0.38	3260	0.17	0.18
1231	0.42	0.52	3300	0.35	0.38
1368	0.00	0.00	3340	0.59	0.64
1482	0.04	0.00	3380	0.72	0.77
1740	0.13	0.28	3420	0.84	0.92
1917	1.20	1.28	3460	0.85	0.90
1943	1.37	1.52	3500	0.91	0.92
2065	5.44	5.29	3540	1.13	1.09
2078	0.00	0.00	3580	1.67	1.55
2159	0.20	0.49	3620	2.55	2.36
2237	0.19	0.38	3660	3.63	3.41
2658	15.15	15.10	3700	3.99	3.89
2700	0.58	0.74	3740	3.56	3.59
2740	0.15	0.15	3780	2.31	2.36
2780	0.05	0.05	3820	1.31	1.35
2820	0.02	0.03	3860	0.89	0.91
2860	0.02	0.03	3900	0.70	0.69
2900	0.03	0.05	3940	0.76	0.72
2940	0.06	0.09	3980	1.12	1.04
2980	0.09	0.15	4020	1.58	1.45
3020	0.10	0.19	4060	2.75	2.59
3060	0.10	0.17	4100	3.72	3.62
4140	3.69	3.56	5060	0.02	0.02
4180	2.99	2.96	5100	0.01	0.01
4220	2.12	2.06	5140	0.00	0.00
4260	1.34	1.32	5180	0.00	0.00
4300	0.91	0.88	5220	0.00	0.00
4340	0.78	0.74	5260	0.00	0.00
4380	0.72	0.69	5300	0.00	0.00
4420	0.69	0.66	5340	0.00	0.00
4460	0.62	0.60	5380	0.00	0.00
4500	0.50	0.50	5420	0.00	0.00
4540	0.32	0.31	5460	0.00	0.00
4580	0.21	0.20	5500	0.00	0.00
4620	0.15	0.15	5540	0.00	0.00
4660	0.12	0.12	5580	0.00	0.00
4700	0.12	0.11	5620	0.00	0.00
4740	0.12	0.11	5660	0.00	0.00
4780	0.12	0.12	5700	0.00	0.00
4820	0.12	0.12	5740	0.00	0.00
4860	0.11	0.11	5780	0.00	0.00
4900	0.10	0.10	5820	0.00	0.00
4940	0.08	0.07	5860	0.00	0.00
4980	0.05	0.05	5900	0.00	0.00
5020	0.03	0.03			

TABLE VI. Feeding distibution obtained for the decay of ^{86}Br (for details see the text).

E [keV]	Feeding (a) [%]	Feeding (b) [%]	E [keV]	Feeding(a) [%]	Feeding (b) [%]
0.0	15.01	20.23	4100	0.04	0.00
1565	3.75	2.84	4140	0.13	0.02
2250	0.00	0.00	4180	0.60	0.19
2350	0.00	0.00	4220	1.95	1.19
2727	2.91	1.77	4260	4.87	4.34
2850	2.34	1.31	4300	9.48	11.34
2917	0.21	0.10	4340	9.02	11.03
2926	1.32	0.58	4380	5.31	5.87
3010	2.95	0.76	4420	1.23	1.05
3099	0.00	0.00	4460	0.28	0.16
3328	3.58	1.52	4500	0.07	0.02
3542	0.18	0.10	4540	0.01	0.00
3580	0.36	0.07	4580	0.00	0.00
3620	0.27	0.05	4620	0.00	0.00
3660	0.30	0.05	4660	0.00	0.00
3700	0.36	0.05	4700	0.00	0.00
3740	0.39	0.04	4740	0.01	0.00
3780	0.36	0.02	4780	0.04	0.00
3820	0.22	0.01	4820	0.09	0.00
3860	0.10	0.00	4860	0.15	0.00
3900	0.06	0.00	4900	0.19	0.01
3940	0.02	0.00	4940	0.16	0.01
3980	0.01	0.00	4980	0.10	0.01
4020	0.01	0.00	5020	0.06	0.01
4060	0.02	0.00	5060	0.04	0.01
5100	0.03	0.01	6140	0.77	0.73
5140	0.05	0.01	6180	1.02	0.96
5180	0.08	0.04	6220	1.05	0.96
5220	0.21	0.12	6260	0.85	0.74
5260	0.63	0.45	6300	0.57	0.48
5300	1.33	1.18	6340	0.35	0.29
5340	2.33	2.41	6380	0.25	0.20
5380	3.40	3.84	6420	0.22	0.18
5420	3.47	4.20	6460	0.23	0.21
5460	2.84	3.34	6500	0.29	0.26
5500	2.06	2.43	6540	0.37	0.34
5540	1.36	1.56	6580	0.42	0.40
5580	0.98	1.09	6620	0.40	0.37
5620	0.78	0.88	6660	0.32	0.28
5660	0.64	0.71	6700	0.21	0.18
5700	0.57	0.62	6740	0.11	0.09
5740	0.48	0.52	6780	0.06	0.05
5780	0.38	0.40	6820	0.03	0.02
5820	0.29	0.31	6860	0.02	0.01
5860	0.21	0.24	6900	0.01	0.01
5900	0.17	0.20	6940	0.01	0.01
5940	0.15	0.18	6980	0.02	0.02
5980	0.16	0.20	7020	0.03	0.03
6020	0.21	0.26	7060	0.05	0.05
6060	0.31	0.38	7100	0.07	0.07
6100	0.51	0.48	7140	0.06	0.06

TABLE VII. Feeding distibution obtained for the decay of ^{86}Br (for details see the text).

E [keV]	Feeding (a) [%]	Feeding (b) [%]	E [keV]	Feeding(a) [%]	Feeding (b) [%]
7180	0.04	0.03	7420	0.00	0.00
7220	0.01	0.01	7460	0.00	0.00
7260	0.00	0.00	7500	0.00	0.00
7300	0.00	0.00	7540	0.00	0.00
7340	0.00	0.00	7580	0.00	0.00
7380	0.00	0.00	7620	0.00	0.00